ORNL-TM-5088

Effects of Tissue Inhomogeneities on Dose Patterns in Cylinders Irradiated by Negative Pion Beams

R. N. Hamm
H. A. Wright
J. E. Turner

OAK RIDGE NATIONAL LABORATORY
OPERATED BY UNION CARBIDE CORPORATION • FOR THE U.S. ATOMIC ENERGY COMMISSION

BLANK PAGE

Printed in the United States of America. Available from
National Technical Information Service
U.S. Department of Commerce
5285 Port Royal Road, Springfield, Virginia 22161
Price: Printed Copy $4.00; Microfiche $2.25

ORNL-TM-5088

Contract No. W-7405-eng-26

HEALTH PHYSICS DIVISION

EFFECTS OF TISSUE INHOMOGENEITIES ON DOSE PATTERNS IN CYLINDERS IRRADIATED BY NEGATIVE PION BEAMS

R. N. Hamm

H. A. Wright

J. E. Turner

This research was partially supported
by the
NATIONAL SCIENCE FOUNDATION

OCTOBER 1975

OAK RIDGE NATIONAL LABORATORY
Oak Ridge, Tennessee 37830
operated by
UNION CARBIDE CORPORATION
for the
U. S. ENERGY RESEARCH AND DEVELOPMENT ADMINISTRATION

ABSTRACT

Effects of the presence of inhomogeneities in tissue irradiated by negative pion beams are investigated. Soft-tissue targets are considered with embedded regions of bone and cavities of air. The absorbed dose is calculated as a function of position in the targets for parallel and converging beams and for two parallel beams that enter the target from opposite sides. Isodose contours are calculated and displayed in each case. While these studies show expected trends, they indicate that specific calculations are needed for other beam parameters and target geometries. The contributions of neutrons to the dose contours can be seen from several calculations made both with and without neutrons.

1. Introduction

The computer program PION-1 (Wright et al. 1975; Turner et al. 1972) was used to study the effects of inhomogeneities on dose patterns in tissue irradiated with negative pions. As plans progress to use pion beams for radiotherapy, calculations related to treatments must take into account regions of different density, such as bone and air cavities, in the body. As described below, calculations were performed for parallel and converging beams as well as two opposed beams that enter the target from opposite sides. The targets consist of soft tissue of unit density, as specified in Table 1, with embedded regions of air and bone. The bone was assumed to have the same relative composition as soft tissue and a density of 2 g/cm^3. Using this approximation for bone introduces an error of no more than a few percent, as discussed in the Appendix.

2. Parallel Beam

2.1 Homogeneous Soft-Tissue Target

In the calculations a uniform, circular, parallel beam of radius 2 cm is incident normally on one end of a tissue cylinder of thickness 30 cm and radius 15 cm. The axes of the beam and cylinder coincide. The dose is computed in thin, concentric cylindrical volume elements about the beam axis with radii of 0.5, 1, 1.5, 2, 3, 4, 5, 7, 10, and 15 cm. The momentum distribution of the pions is assumed to be Gaussian, with a mean value of 153 MeV/c (mean energy = 67 MeV) and a spread of 2% (i.e., one-half of the incident pions have momentum within 2% of the mean). The mean range of the pions in soft tissue is 15 cm, which is one-half the thickness of the target.

Figure 1 shows the calculated isodose contours in the homogeneous soft-tissue target. Pions enter from the left, where the beam axis passes through the zero position on the vertical scale. The contours have cylindrical symmetry about this axis. Depth (cm) in the target is marked on the horizontal scale and distance (cm) from the beam axis on the vertical scale. Contours are shown at locations where, in terms of the peak dose, the dose levels are 0.9, 0.8, 0.5, 0.2, 0.1, 0.05 and 0.01. The value of the peak dose, 1.79×10^{-8} rad per incident pion, is indicated in the upper right-hand corner of Fig. 1. The computer program ISODATA (Anderson et al. 1974) was used to calculate the locations of the contours from the raw Monte Carlo dose data; the graphics package ORGRAPH (Nestor et al. 1974) was used to plot the contour points.

The dose contours spread as the beam enters the target primarily because of multiple Coulomb scattering (Hamm et al. 1975), but also because of the nuclear reactions of the pions. About 85% of the incident pions come to rest in the target (Turner et al. 1972), mostly in the region between 14 and 16 cm, before being absorbed by a nucleus. The contours show the peaking of the dose in this area. The spread of the dose contours is increased in the stopping region due to the transport of energy away from the capture sites by the secondary particles produced.

Neutrons are the principal particles that transport energy large distances away from the capture region. To see their effect, the calculations were repeated with neutron interactions ignored. The resulting contours are shown in Fig. 2. The levels for 5% of the peak

dose and greater have practically the same locations as in Fig. 1. The 1% level extends out to a distance of 4.9 cm in the peak region with neutrons and 4.6 cm without neutrons. The peak dose is reduced by 4.5% when neutrons are ignored.

The dose contours were computed from the histories of 10^4 incident pions and the secondary particles they produce. The calculations were performed on the IBM 360 Model 91 computer in approximately 8 minutes, the major portion ($\sim$ 5.5 minutes) being required to handle neutrons. Comparison of Figs. 1 and 2 indicates that very little error is made in locating isodose contours around the peak region from calculations that ignore neutrons. The computing time is thereby reduced by a factor of two-thirds.

Except for Fig. 2 and Fig. 5, below, neutrons are included in all calculations reported here.

2.2 Soft Tissue with Bone

The target was next provided with a circular, cylindrical volume of bone (density 2 g/cm^3 and composition of Table 1) with radium 1 cm, centered on the beam axis between the depths 1 cm and 3 cm. The calculated absorbed dose contours are shown in Fig. 3, where the cross hatching indicates the region occupied by bone. The beam is the same as that used for the homogeneous soft-tissue target, and so a comparison of Figs. 3 and 1 shows the effects of the presence of the bone on the dose pattern. The contours behind the bone region generally lie at shallower depths. The depth of the 90% contour, for example, is reduced by about 2 cm with the bone present.

The peak dose, which occurs at a depth of 14.5 cm in Fig. 1, is located at a depth of 13 cm in Fig. 3. The value of the peak dose is reduced from 1.79×10^{-8} in Fig. 1 to 1.46×10^{-8} rad per pion in Fig. 3. Bone increases the amount of multiple Coulomb scattering, which spreads the region through which the pions stop.

Figure 4 shows the dose contours obtained when the bone cylinder is located at a greater depth, between 10 cm and 12 cm, close to where many of the pions stop. The effects are more marked with the deep bone in Fig. 4 than in Fig. 3, where the bone is nearer the surface. Whereas only the lowest dose contours in Fig. 3 have concave portions at depths beyond the peak, the contours in Fig. 4 for 50% and below are concave. The peak dose in Fig. 4 is 1.94×10^{-8} rad per pion. In this case, the bone's being directly in front of the stopping region causes it to become somewhat compressed.

The calculations for Fig. 4 were rerun with neutron interactions ignored. The results are shown in Fig. 5. The dose contours for 5% and greater are practically indistinguishable in the two cases. The locations of the 1% contours are within 0.5 cm of each other. The peak dose without neutrons is reduced about 4%. The effects of ignoring neutrons in this example with bone present appear to be comparable to those found for homogeneous soft tissue (Figs. 1 and 2).

Figures 6, 7, and 8 give results when elongated cylindrical regions of bone of different radii (0.25, 0.50, and 1.0 cm) are present. The patterns in Figs. 6 and 7 do not differ greatly, as one might expect with

only the thin piece of bone present, although their concave shape on the beam axis is clearly evident in Fig. 6. The contrast between Figs. 7 and 1 and Figs. 8 and 1 is greater. The dose pattern is no longer monatonic; additional closed contours appear in the region around 10 cm depth. Increasing the amount of bone increases multiple Coulomb scattering and causes more nuclear reactions. Comparison of Figs. 1, 6, 7, and 8 shows the steady decrease in the magnitude of the peak dose and the increasing diffuseness of the dose patterns with more and more bone present. There does not appear to be a simple rule for scaling from one case to another.

An additional calculation was made with an annular cylindrical ring of bone, centered on the beam axis between 10 and 12 cm. The inner and outer radii of the annulus were chosen to be 0.5 and 1.0 cm. The calculated isodose contours are presented in Fig. 9. The annulus causes the shape of the peak to change somewhat, but does not change the peak dose when compared with Fig. 1. The maximum dose occurs at a depth of about 13.5 cm in Fig. 9 compared with 14.5 cm when no bone is present.

2.3 Soft Tissue with Air

Examples with cylindrical air cavities at atmospheric pressure in soft tissue are presented in Figs. 10-14. Comparison of Figs. 10 and 1 indicates that the depth of the peak is increased by about 1 cm because of the air cavity between 1 and 3 cm. The peak dose is reduced by 4% because of the air. In Fig. 11, where the air cavity is located deeper in the target, the peak occurs at an even greater depth and the peak dose is reduced by over 13%. As with the bone, the general effect of the

inhomogeneity is to make the dose pattern more diffuse. The effect is larger when the inhomogeneity is near the pion stopping region than when it is near the surface of the irradiated target.

The elongated air cavities along the axis in Figs. 12-14 have an even more marked effect. The total volume of air in Figs. 10 and 11 is 6.3 cm^3 compared with 0.98, 3.9, and 15.7 cm^3 in Figs. 12, 13, and 14. It is thus apparent that the elongation of an inhomogeneity is critical in determining dose patterns, even when the geometric shape--in these examples, a right circular cylinder--and the amount of matter traversed are the same. There does not appear to be any reliable way of scaling from one example to another.

2.4 Soft Tissue with Bone and Air

We present one example for the parallel beam incident on soft tissue that contains both bone and air in circular cylindrical regions on the beam axis. In Fig. 15 the bone is located between 1 and 3 cm and the air between 10 and 12 cm. The radius of both cylinders is 1 cm. Compared with the homogeneous target, the two regions in Fig. 15 tend to compensate in that the total nuclear cross sections seen by the pions are almost identical in Figs. 1 and 15. Near the surface, however, the bone introduces a relatively large amount of multiple Coulomb scattering, which spreads the dose pattern. The peak dose in Fig. 15 is 1.37×10^{-8} rad per pion.

3. Converging Beam

3.1 Homogeneous Soft-Tissue Target

A completely convergent beam is next considered. As before, all of the pions enter the target uniformly over a circle of radius 2 cm. Instead of traveling parallel to the beam axis, however, each pion as it enters the target, is initially directed toward a point on the axis located at a depth of 15 cm. Multiple scattering deflections and nuclear reactions cause the beam to spread as it penetrates the target. This case represents the ultimate focusing of a beam of this size and momentum distribution. A few examples with the beam will be shown in this section.

The dose pattern for the convergent beam incident on the homogeneous soft-tissue target is shown in Fig. 16. The dose contours are much more concentrated than they are in Fig. 1 for the parallel beam. The peak dose of 5.52×10^{-8} rad per pion with the convergent beam is three times greater than the peak dose with the parallel beam in Fig. 1. The maximum doses in both cases occur at about the same depth.

3.2 Soft Tissue with Bone

Figure 17 shows the dose pattern from the convergent beam when a bone cylinder of radius 1 cm is present between 10 and 12 cm. The peak dose of 8.21×10^{-8} rad per pion occurs about 2 cm closer to the surface compared with the homogeneous target Fig. 16. There is less lateral spread of the contours with the bone present.

3.3 Soft Tissue with Air

The contours with an air cylinder between 10 and 12 cm are given in Fig. 18. They are spread considerably more than in Fig. 16, and the peak dose is 3.72×10^{-8} rad per pion.

3.4 Soft Tissue with Bone and Air

Calculations were also performed for the converging beam with both bone and air cylinders in the target simultaneously, the bone between 1 and 3 cm and the air between 10 and 12 cm. The resulting contours are shown in Fig. 19.

4. Quantitative Comparison of Parallel and Converging Beams

Table 2 summarizes the peak doses per pion for the parallel and converging beams incident on the same configurations--a homogeneous soft-tissue target and soft-tissue targets with bone and/or air cylinders of radius 1 cm on the beam axis. The last column of the Table presents the ratios of the peak doses for the converging and parallel beams. In the homogeneous soft-tissue target, the peak dose is increased by a factor of 3.1 by changing from a parallel to a converging beam. All other factors are the same: the momentum distribution of the pions and the area over which they are uniformly incident. It is interesting to note that the bone enhances the ratio to 4.2 while the air lowers it to 2.4. The bone reduces the size of the volume in which the pions stop, while the air increases it.

5. Opposed Parallel Beams

5.1 Homogeneous Soft-Tissue Target

An identical, but directly opposed parallel beam, incident on the 30 cm target from right to left along the same axis, was added to the beam of Fig. 1. The resulting contours are shown in Fig. 20. Since the beams are identical, the figure is symmetric. The mean range of the incident pions, 15 cm, is one-half the thickness of the target. The enhanced peaking of the dose distribution at the center of the target and consequent reduction of the relative surface dose achieved with the opposed beams are evident from a comparison of Fig. 20 with Fig. 1. The 0.5 level, which intersects the beam axis at a depth near 12.5 cm in Fig. 1, crosses the axis at a depth of 13.2 cm in Fig. 20. The 0.2 level, which does not intersect the beam axis on the left side of Fig. 1, intersects it near 11 cm in Fig. 20. The peak dose in Fig. 20 is 3.17×10^{-8} rad per pion. Compared with the single-side irradiation in Fig. 1, the peak-to-surface dose ratio is almost doubled by irradiating from the two opposing directions.

5.2 Soft Tissue with Bone

Figure 21 shows the opposed beam case with a circular cylinder of bone of radius 1 cm located on the beam axis between 1 and 3 cm. There is no bone on the right, and so the figure is assymetric with respect to left and right. Compared with Fig. 20, the peak dose is reduced to 2.76×10^{-8} rad per pion and the dose pattern is more diffuse.

5.3 Soft Tissue with Air

Figure 22 shows the contours with a cylindrical air cavity between 1 and 3 cm depth on the left side. The air allows more pions from the left to travel past the mean range of 15 cm in soft tissue. As a result, a higher peak dose of 3.45×10^{-8} rad per pion occurs around 15.5 cm.

6. Conclusions

These studies illustrate some effects of inhomogeneities on dose patterns in targets irradiated by negative-pion beams. It is clear that the presence of bone, air cavities, and other regions of different density must be taken into account in planning therapeutic treatments with negative pions. The general nature of the differences in dose patterns with and without inhomogeneities can be understood qualitatively. The examples shown here indicate that it is difficult to extrapolate from one case to another, even for the same pion beam. On the other hand, a Monte Carlo code such as PION-1 can provide detailed calculations rapidly without undue cost, especially if neutrons are not always included.

APPENDIX

The approximation introduced by using soft tissue of density 2 g/cm^3 to represent bone is good to within a few percent for calculating dose. The relative composition given in Table 1 is the same as that used for soft tissue of density 0.961 g/cm^3 in an earlier study (Turner et al. 1968) of the effects of the presence of bone in targets irradiated by nucleons with energies of several hundred MeV. The relative composition of bone used in that investigation is given in Table 3, wet bone with a density of 1.96 g/cm^3 being assumed. Comparison of Tables 1 and 3 shows the differences between the two media. The four elements, hydrogen, oxygen, carbon, and nitrogen, which are assumed to comprise soft tissue, account for 96.4% of the atoms in wet bone, the remaining 3.6% consisting of heavier atoms.

Bone deposition by pions occurs as a result of interactions with atomic electrons and with atomic nuclei. The mass stopping powers of soft tissue and wet bone for pions with energies up to 80 MeV are almost equal, since the relative compositions are so similar. The dose deposited as a result of interactions with atomic electrons is thus nearly identical in the two media. Because of the larger nuclear sizes of the heavier atoms in bone, more nuclear reactions will occur per g/cm^2 traveled by a pion in bone than in soft tissue. Furthermore, each reaction with a heavier element will, on the average, produce a larger number of secondary particles than a reaction with a lighter element. However, the energy available to these secondary particles from an incident pion is the same in both bone and soft tissue, and so the different multiplicity will not cause the dose to be greatly different.

An estimate of the dose difference in bone and in soft tissue, having the same density as bone, can be made from a comparison of their relative atomic densities. At a given pion energy, the reaction cross section for a nucleus of mass number A is proportional to the geometrical cross section of the nucleus, which in turn is proportional to $A^{2/3}$. The average atomic mass number of the heavier atoms in bone is about 35. Compared with oxygen, the most abundant element in soft tissue after hydrogen, the microscropic cross sections of the heavier elements in bone are greater by a factor of the order of $(35/16)^{2/3} = 1.69$. Since 3.6% of the atoms in bone have the larger cross sections, the macroscopic cross section in bone, expressed in cm^2/g, is larger than that in soft tissue by a factor of about $0.964 + 0.036 \times 1.69 = 1.025$. Differences of no more than a few percent are thus expected between pion doses calculated for bone and for soft tissue with the same density as bone.

This expectation is borne out by calculations for a broad beam of pions, incident normally on a semi-infinite soft-tissue slab, containing a section of bone between two planes parallel to the slab surfaces (Santoro et al. 1974). The dose, plotted as a function of depth in the slab expressed in g/cm^2, with the bone section present is indistinguishable from that calculated when the bone is replaced by soft tissue.

TABLE 1

Composition of Unit-Density Tissue Used in Calculations

(From Turner et al. 1968)

Element	Atomic Density (atoms per cm^3)	Relative Atomic Density (percent)
Hydrogen	6.22×10^{22}	63.2
Oxygen	2.55	25.9
Carbon	0.940	9.5
Nitrogen	0.134	1.4

TABLE 2

Comparison of Peak Doses (in units of 10^{-8}) rad per incident pion) for Parallel and Converging Beams on Various Target Configurations

Target	Parallel Beam		Converging Beam		Ratio of Peak-Doses
	Peak Dose	Figure	Peak Dose	Figure	
Homogeneous Soft Tissue	1.79	1	5.52	16	3.1
Tissue with Bone 10-12 cm	1.94	4	8.21	17	4.2
Tissue with Air 10-12 cm	1.55	11	3.72	18	2.4
Tissue with Bone 1-3 cm and Air 10-12 cm	1.37	15	3.43	19	2.5

TABLE 3

Relative Composition of Bone

(From Turner et al. 1968)

ELEMENT	RELATIVE ATOMIC DENSITY (percent)
Hydrogen	56.8
Carbon	20.0
Oxygen	17.7
Nitrogen	1.9
Calcium	1.8
Phosphorus	1.6
Sodium	0.1
Sulfur	0.05
Magnesium	0.04
Potassium	0.03

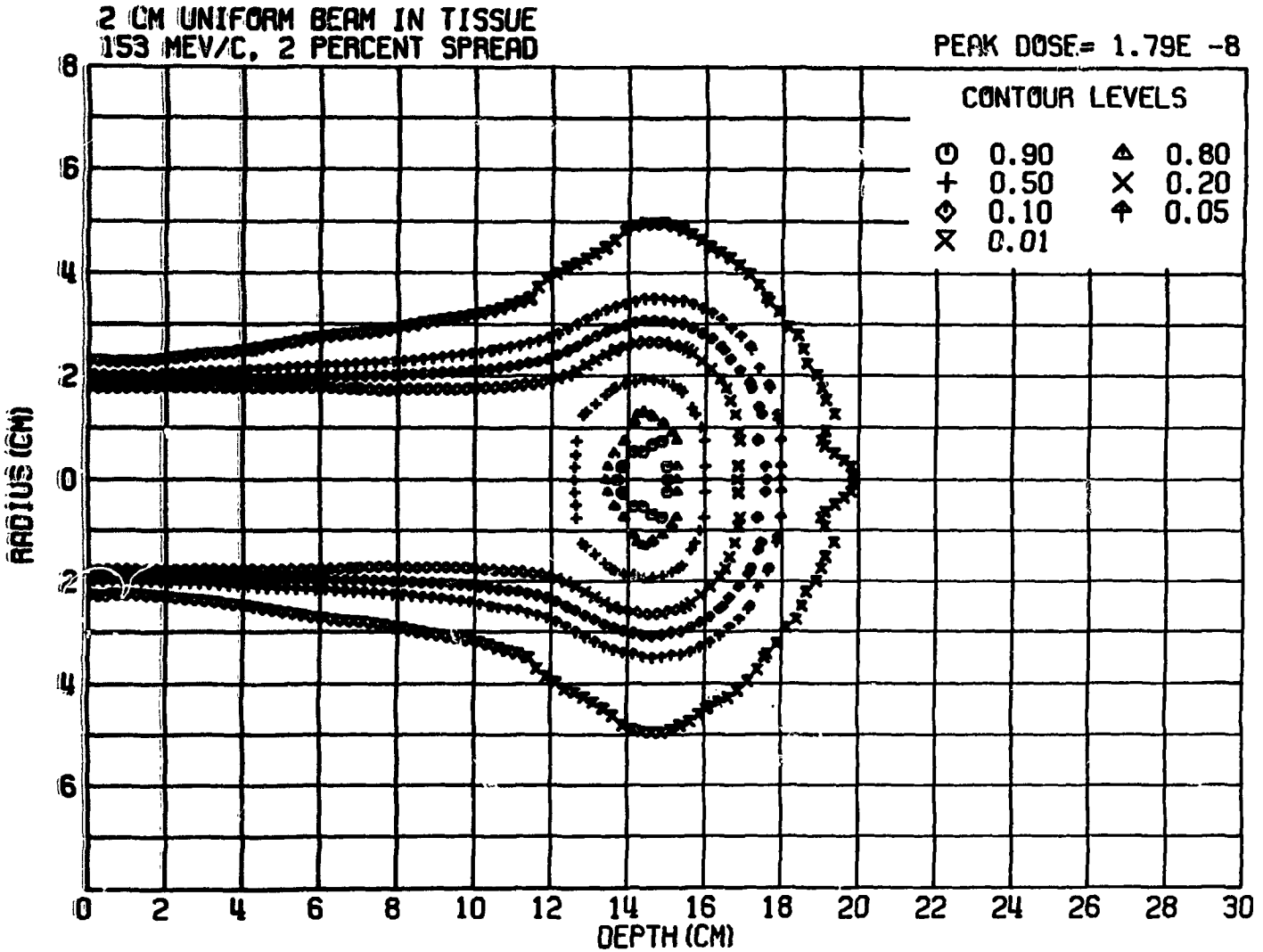

Fig. 1 - Isodose contours for parallel beam incident on homogeneous soft-tissue target. Distances are in cm.

ORNL-DWG 75-12554

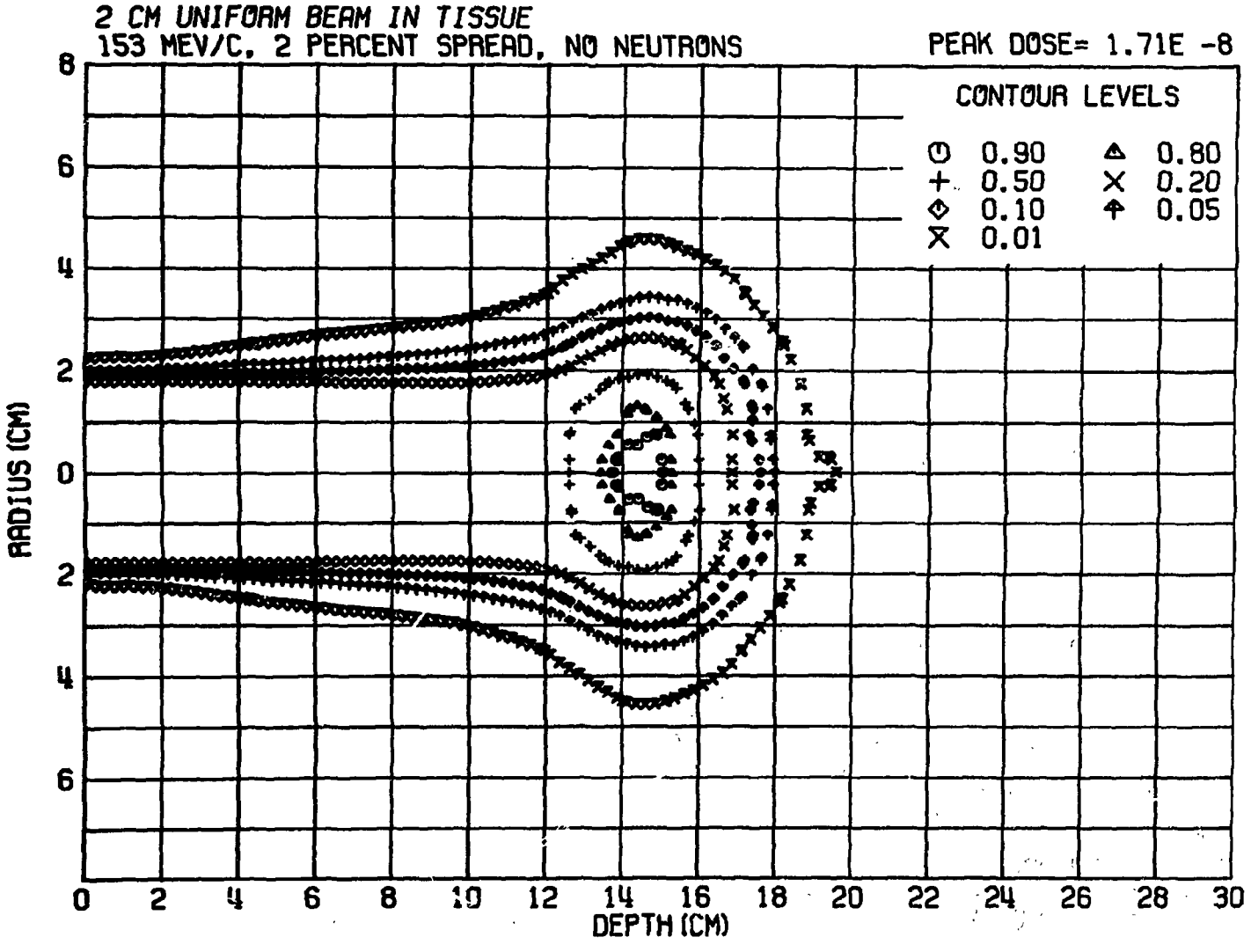

Fig. 2 - Isodose contours with neutron interactions ignored

ORNL-DWG 75-12555

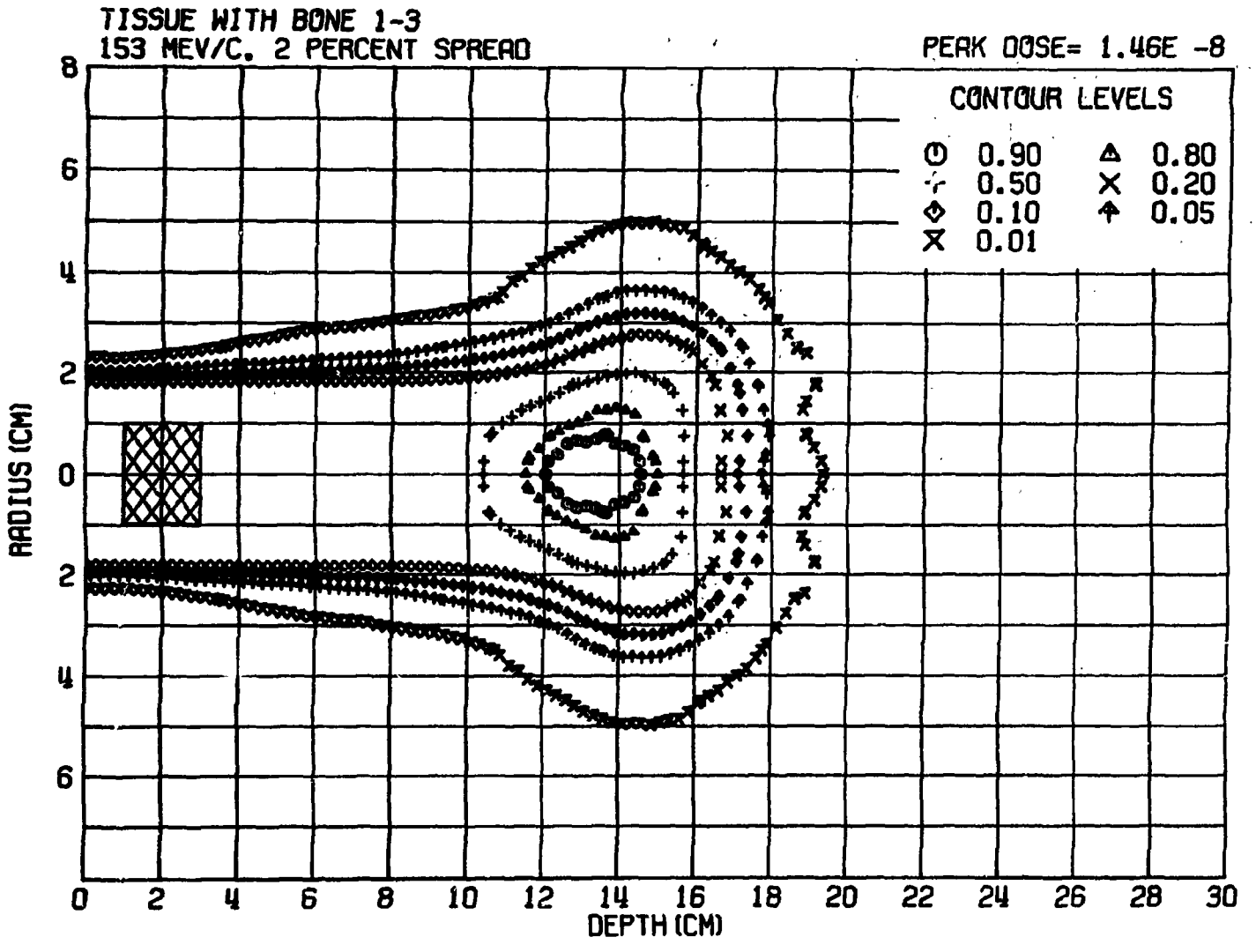

Fig. 3 - Isodose contours in tissue with bone in the circular cylindrical region of radius 1 cm indicated by the cross hatching between 1 and 3 cm.

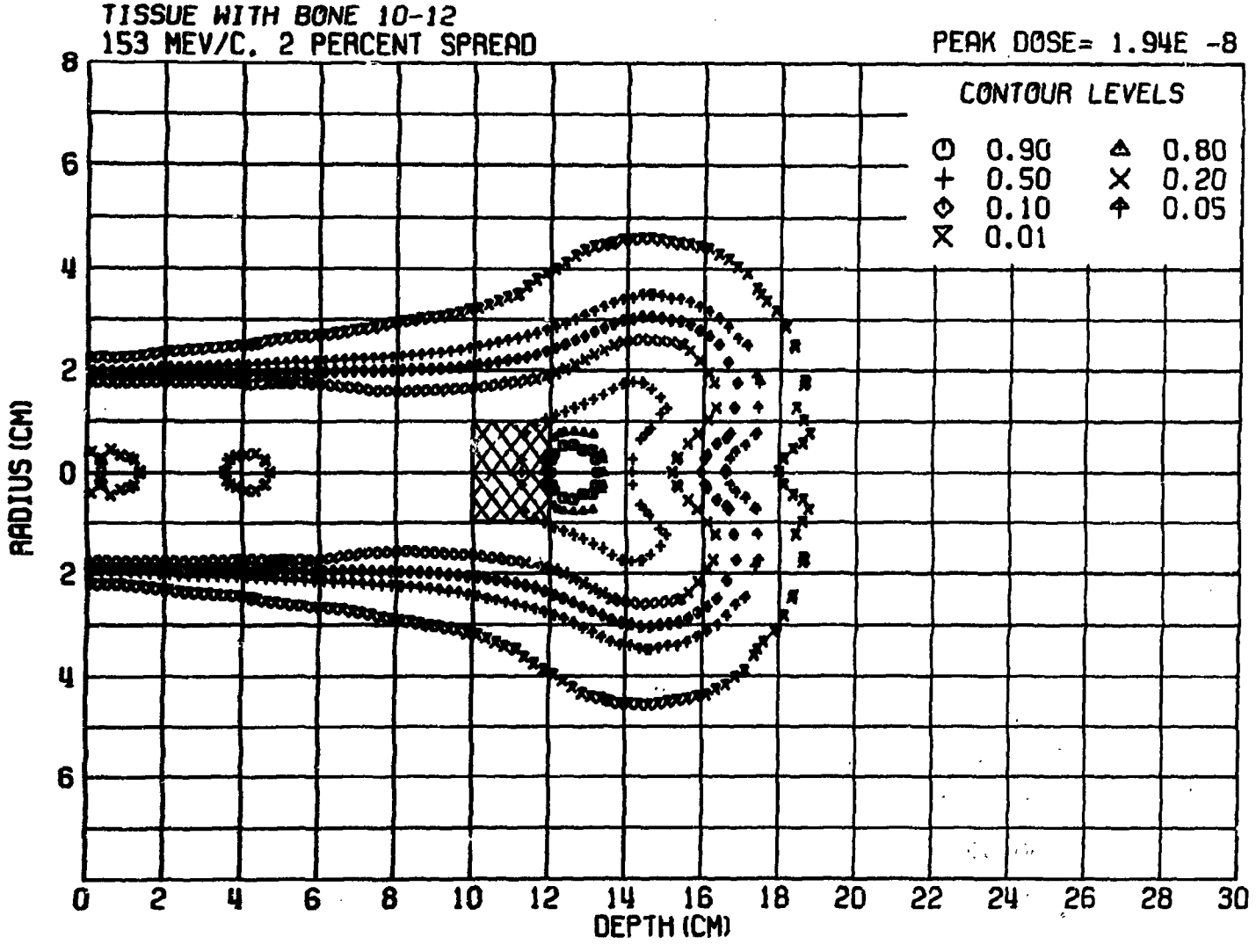

Fig. 4 - Isodose contours with bone cylinder between 10 and 12 cm.

ORNL-DWG 75-12557

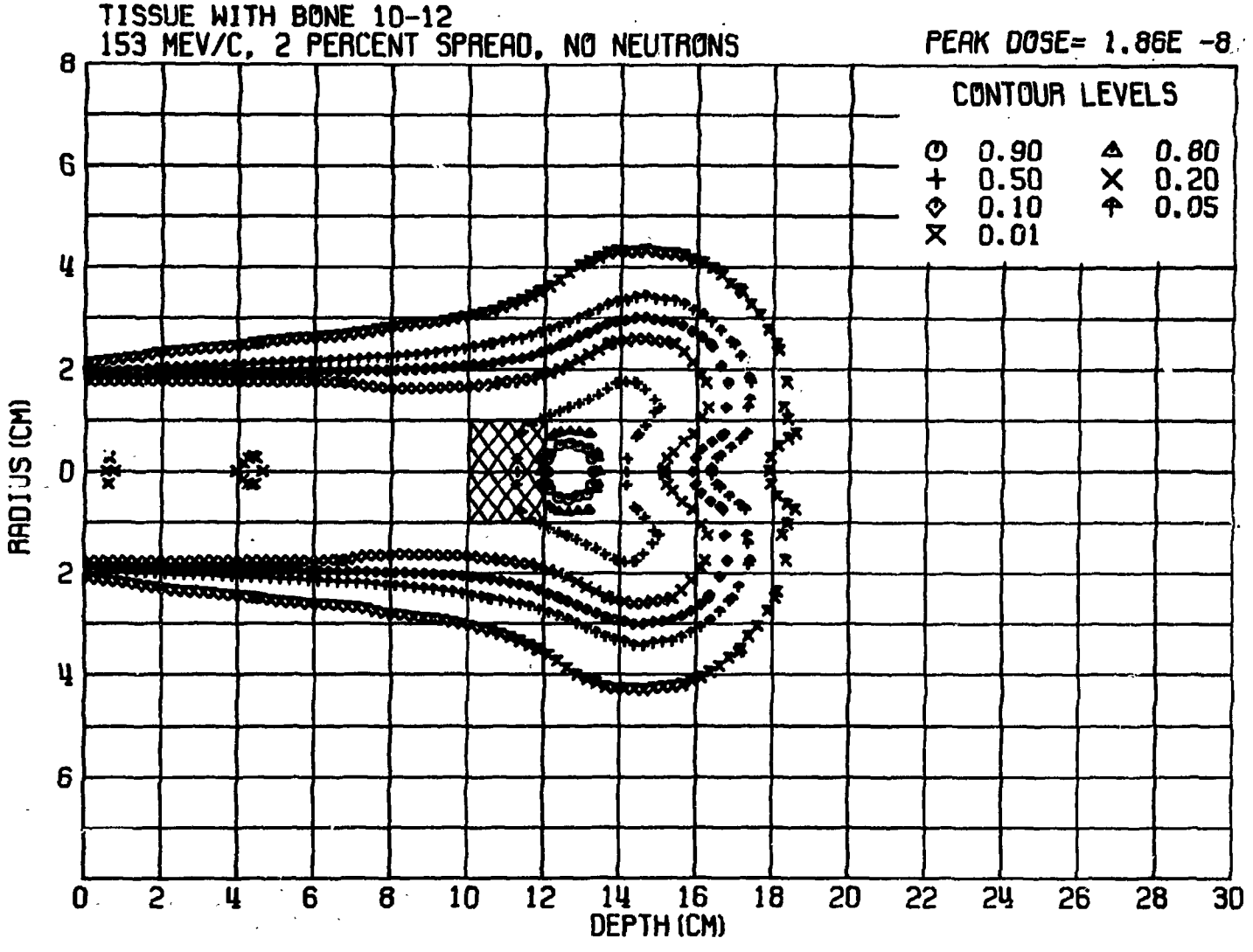

Fig. 5 - Isodose contours with bone cylinder between 10 and 12 cm and neutron interactions ignored.

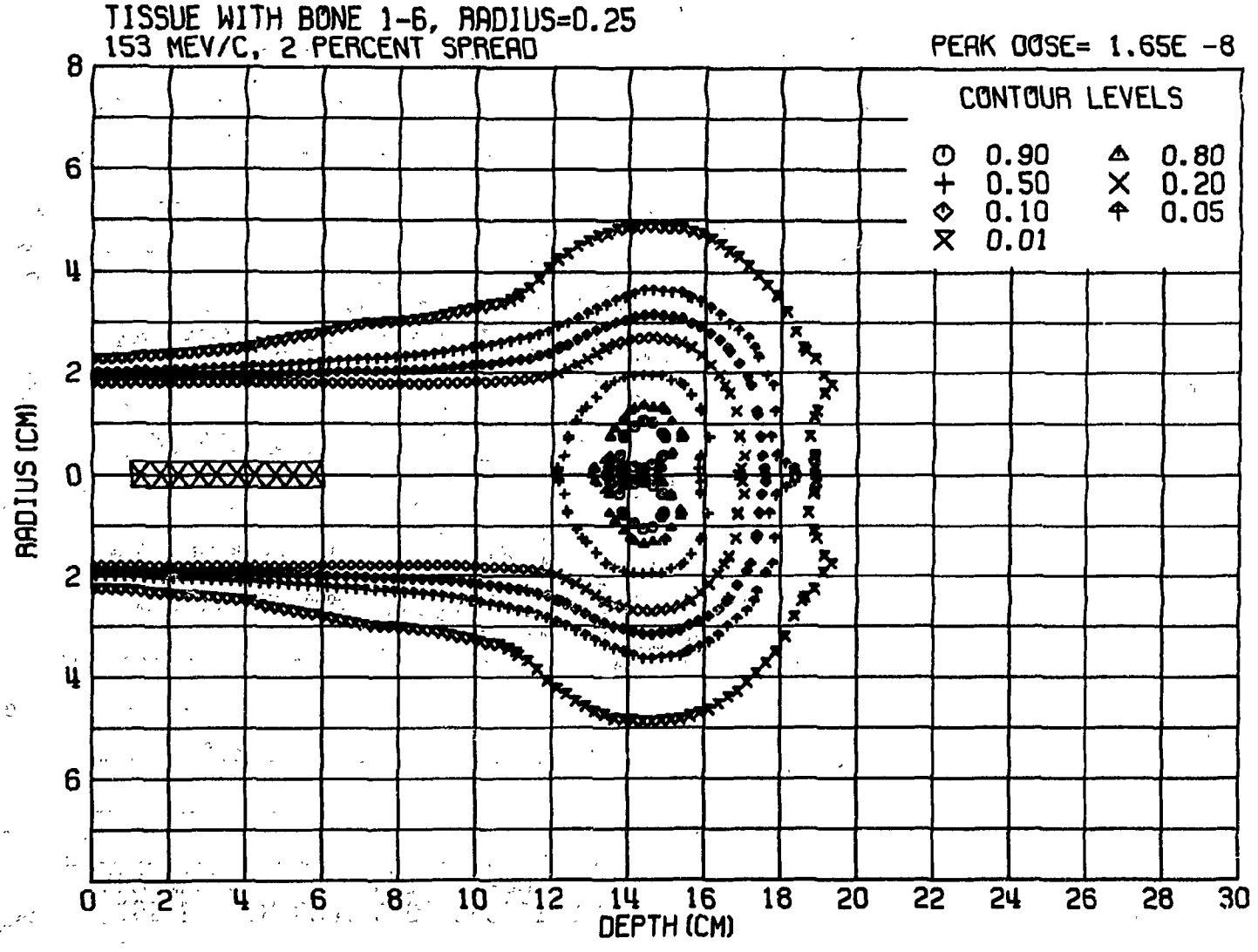

Fig. 6 - Isodose contours with bone cylinder of radius 0.25 cm between 1 and 6 cm.

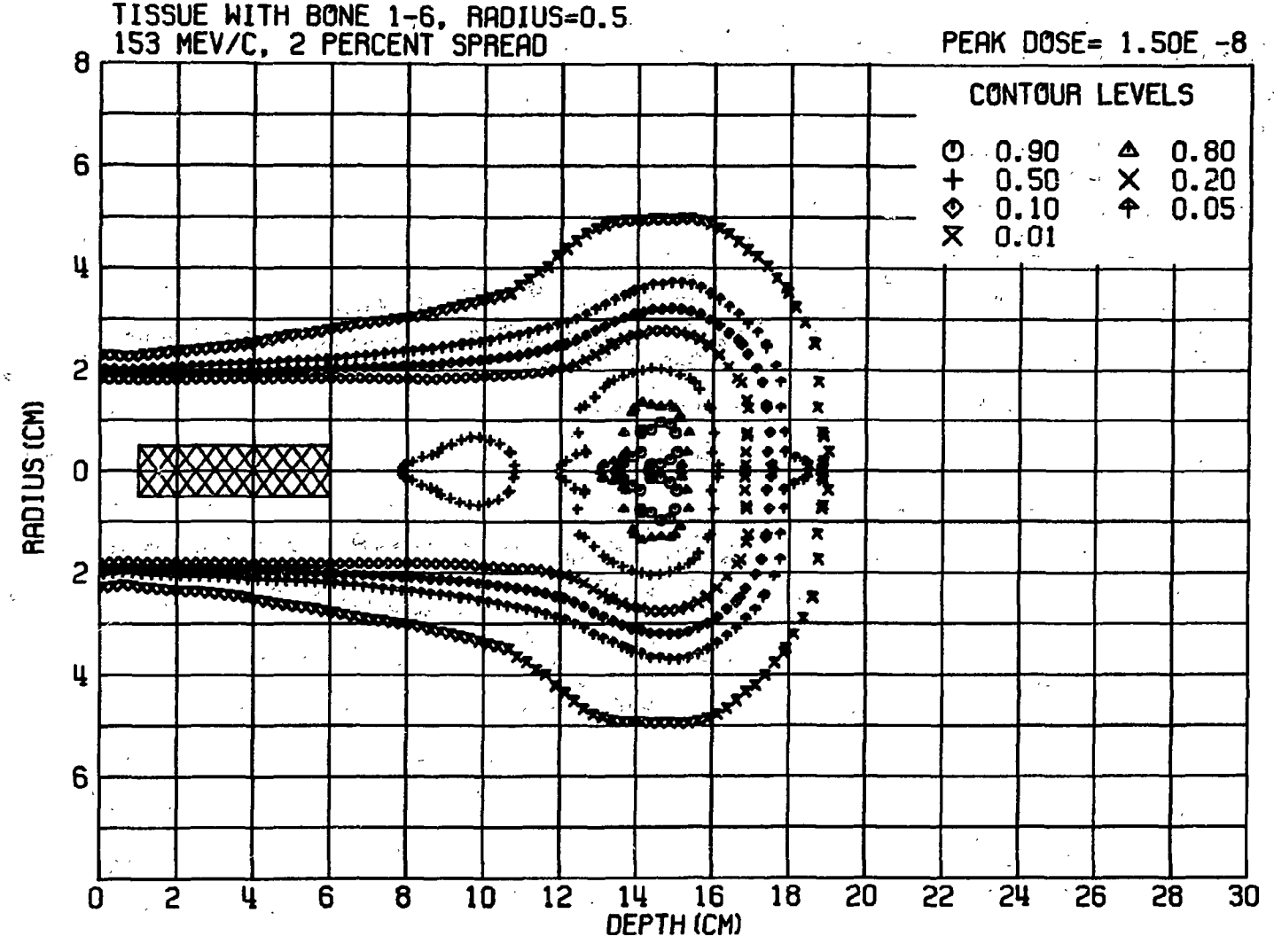

Fig. 7 - Isodose contours with bone cylinder of radius 0.50 cm between 1 and 6 cm.

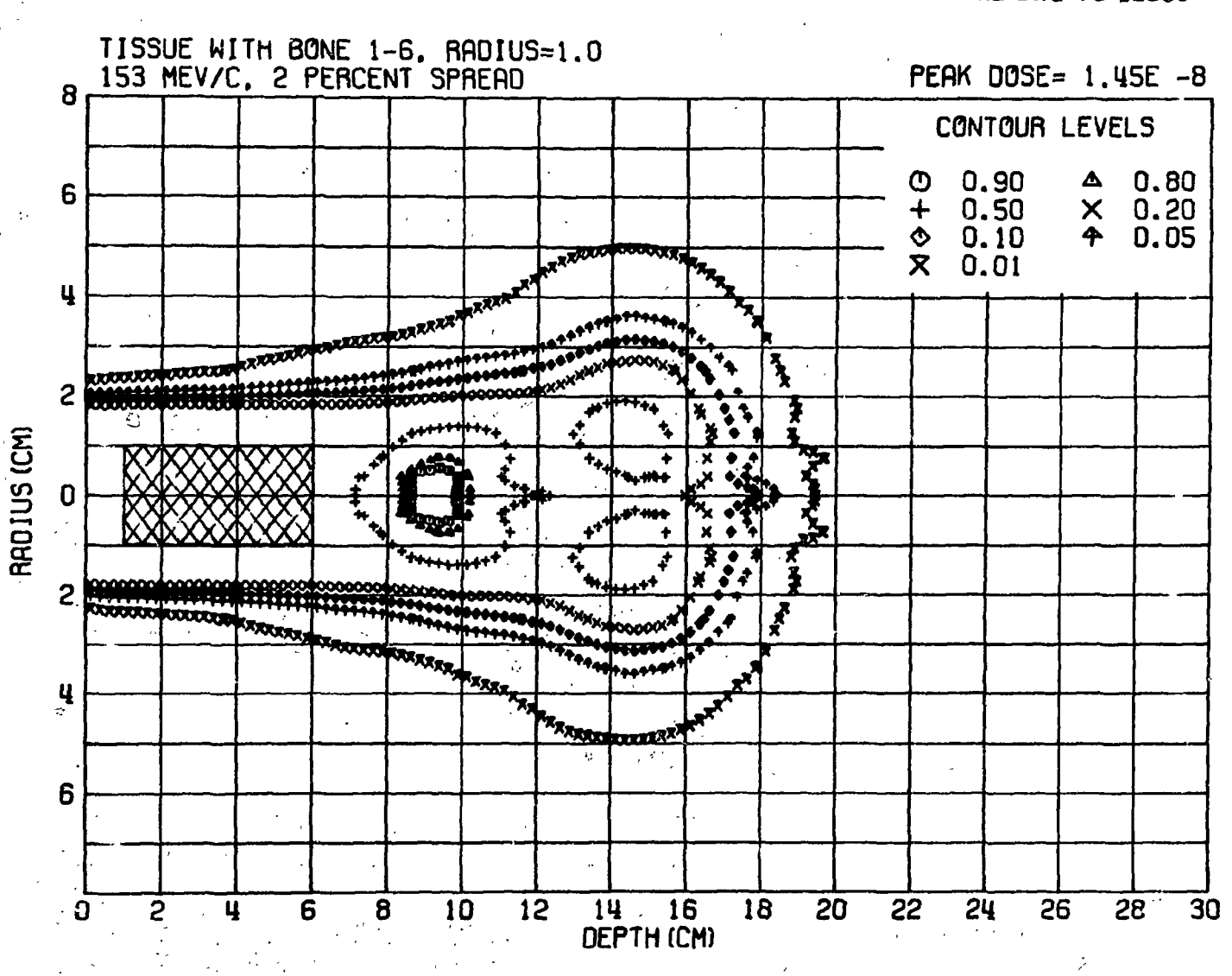

Fig. 8 - Isodose contours with bone cylinder of radius 1.0 cm between 1 and 6 cm.

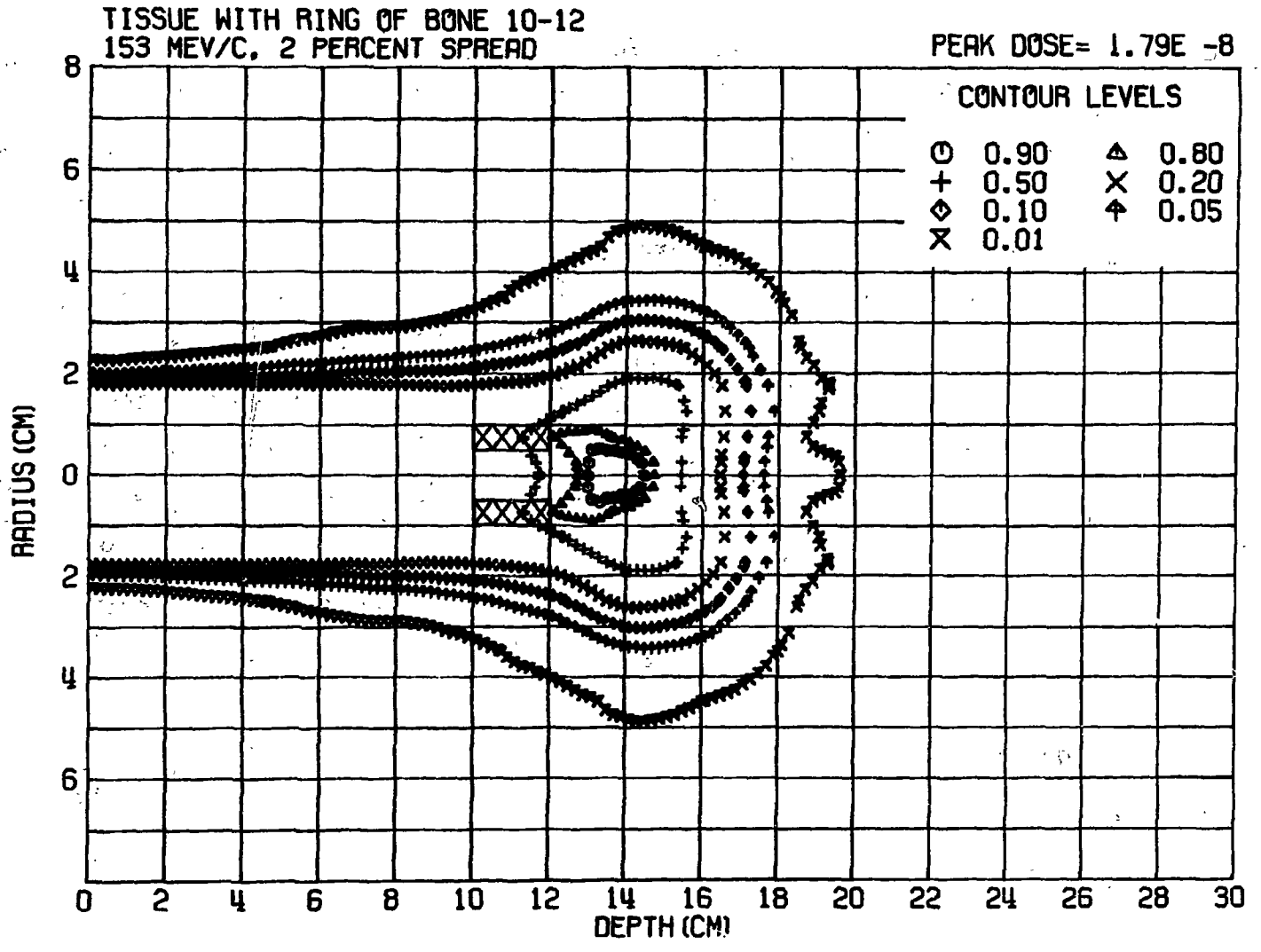

Fig. 9 - Isodose contours with annular bone cylinder of inner radius 0.5 cm and outer radius 1.0 cm between 10 and 12 cm.

ORNL-DWG 75-12562

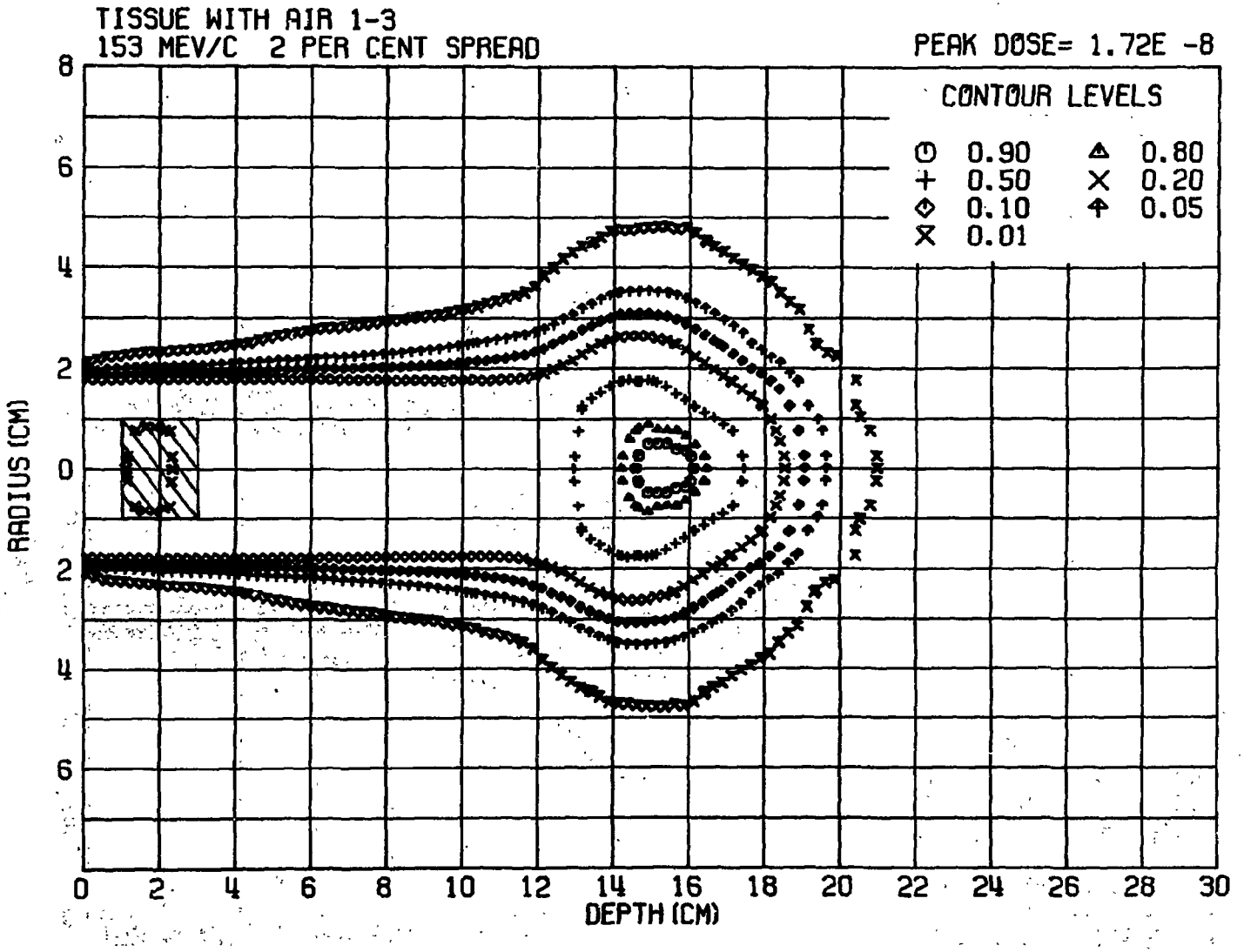

Fig. 10 - Isodose contours in tissue with air cylinder of radius 1 cm between 1 and 3 cm.

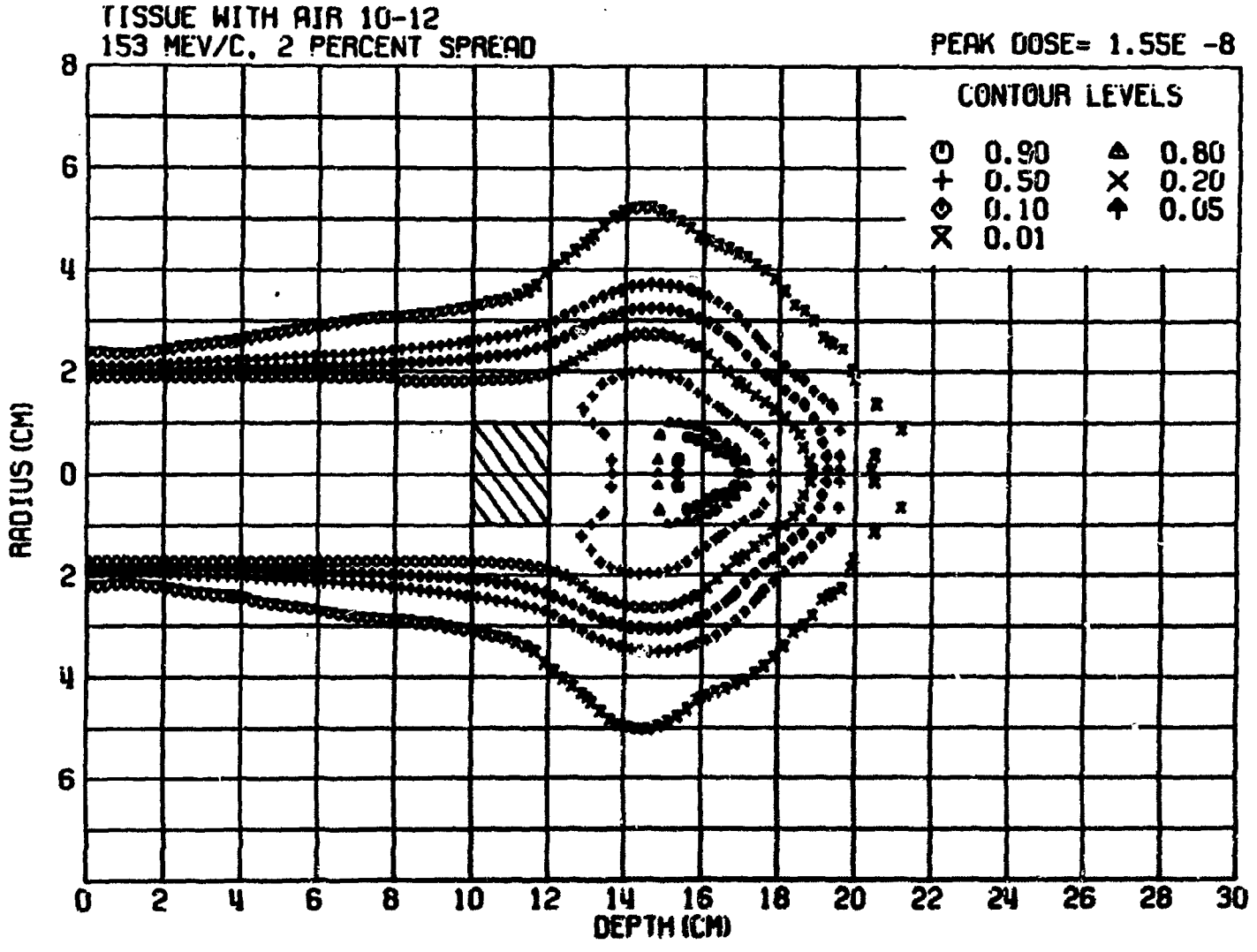

Fig. 11 - Isodose contours with air cylinder between 10 and 12 cm.

ORNL-DWG 75-12564

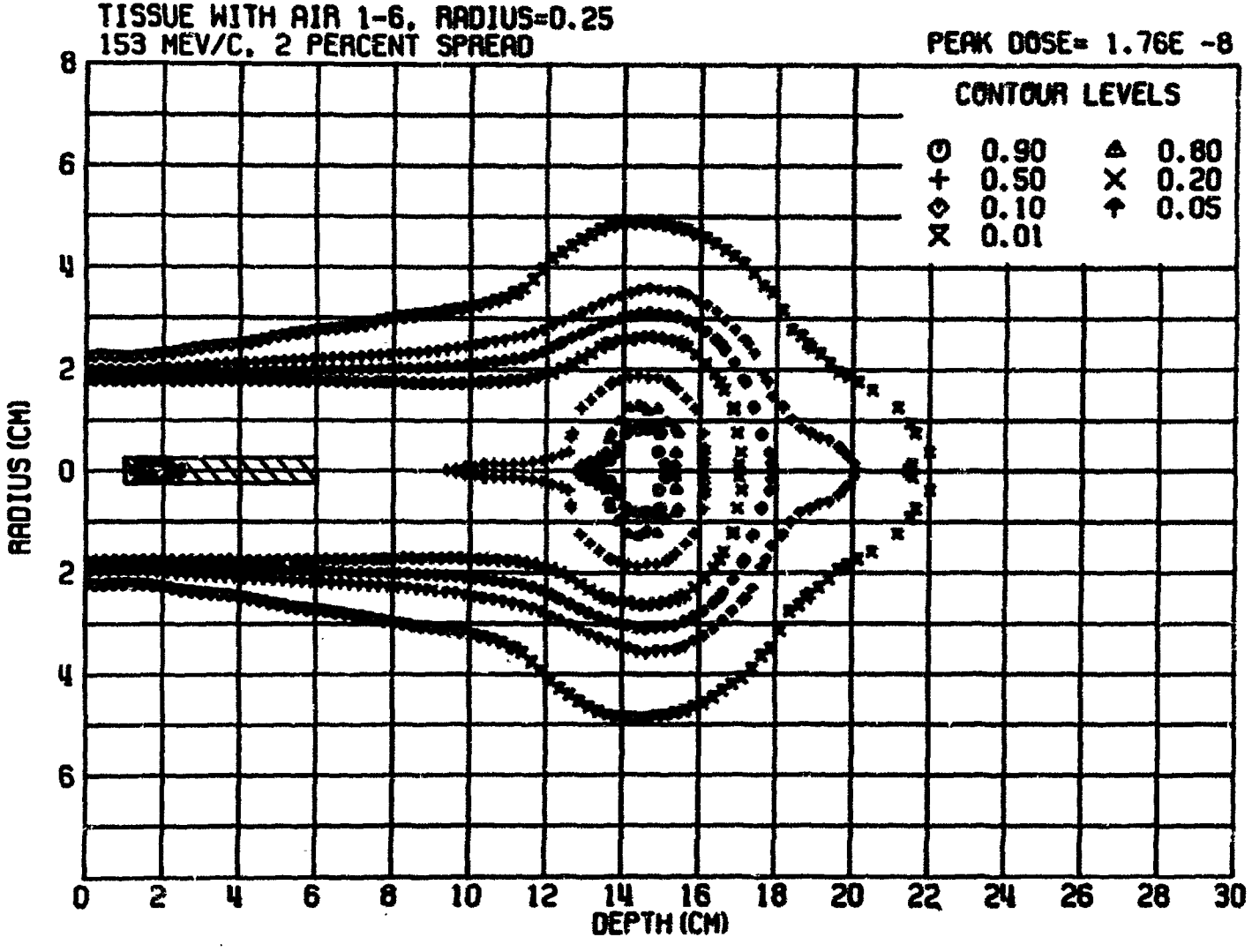

Fig. 12 - Isodose contours with air cylinder of radius 0.25 cm between 1 and 6 cm.

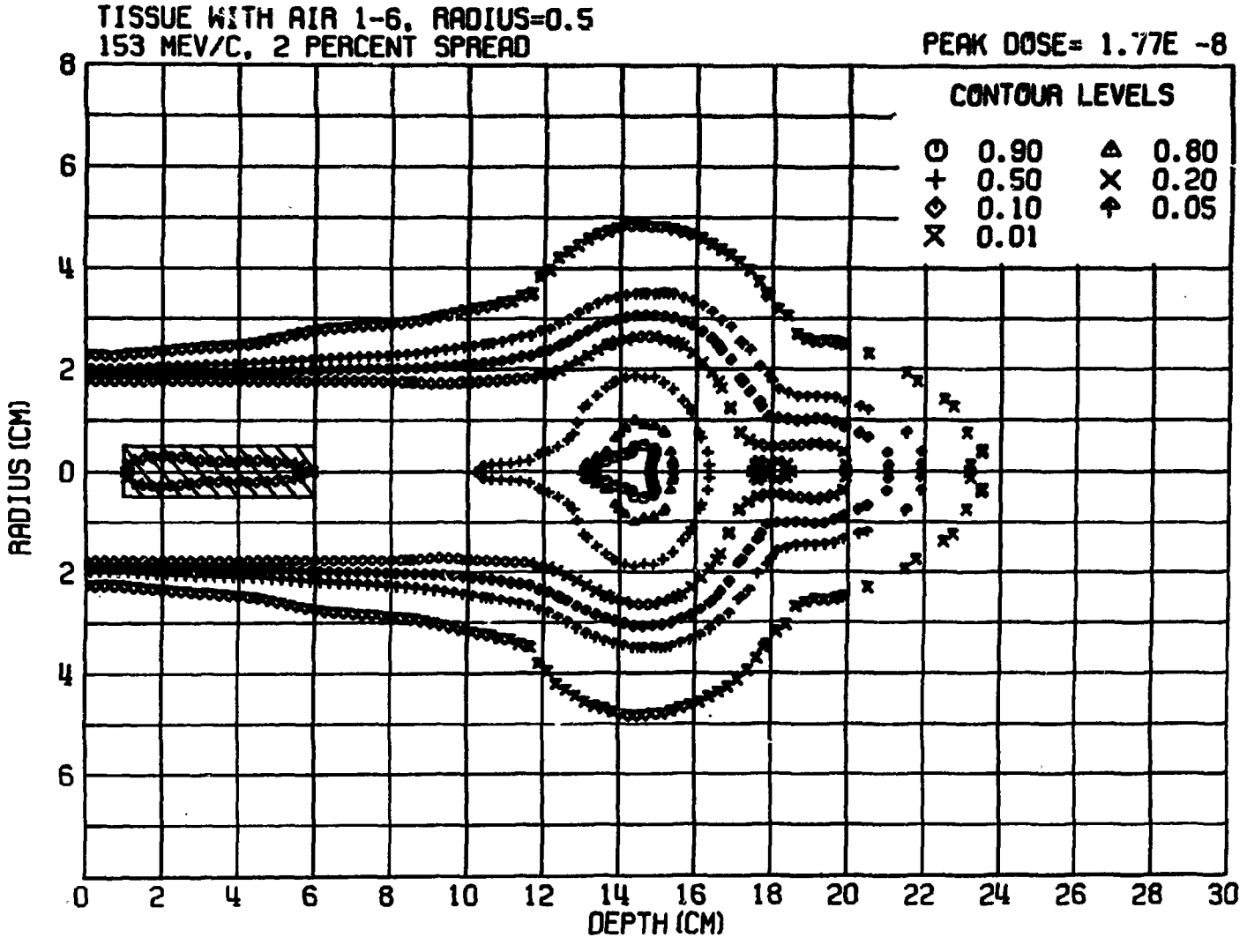

Fig. 13 - Isodose contours with air cylinder of radius 0.50 cm between 1 and 6 cm.

ORNL-DWG 75-12566

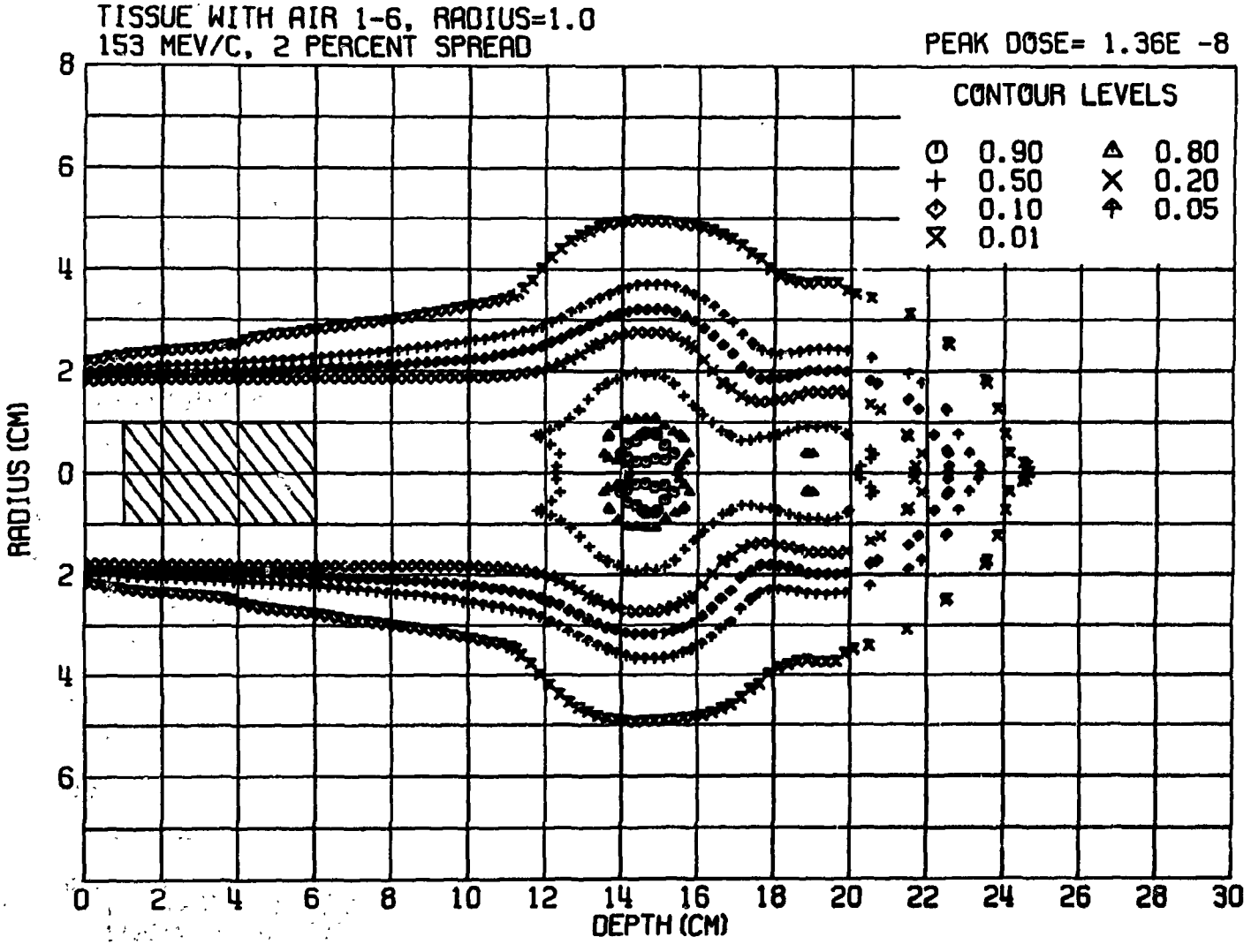

Fig. 14 - Isodose contours with air cylinder of radius 1.0 cm between 1 and 6 cm.

ORNL-DWG 75-12567

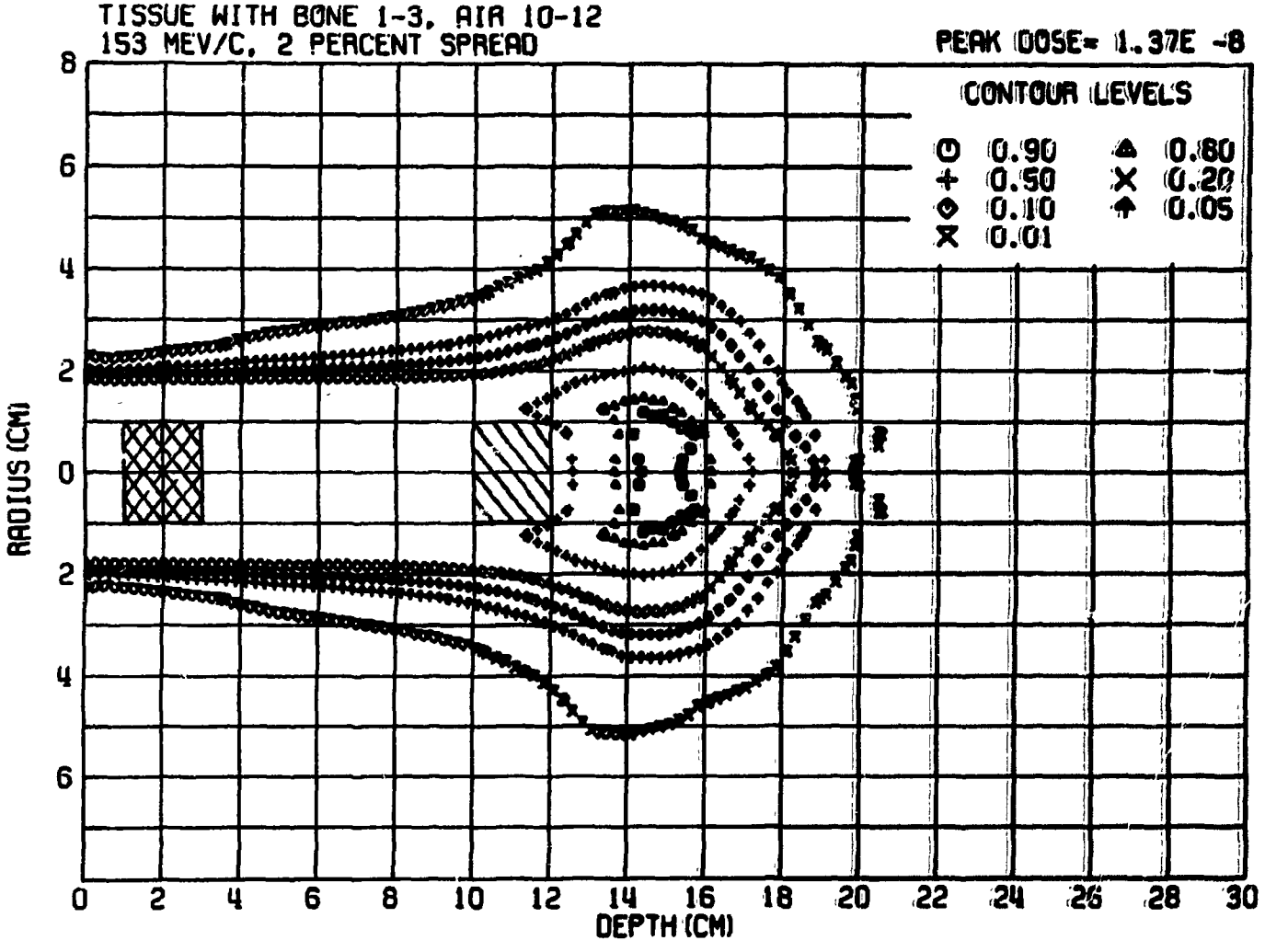

Fig. 15 - Isodose contours with bone cylinder of radius 1 cm between 1 and 3 cm and air cylinder of radius 1 cm between 10 and 12 cm.

ORNL-DWG 75-12568

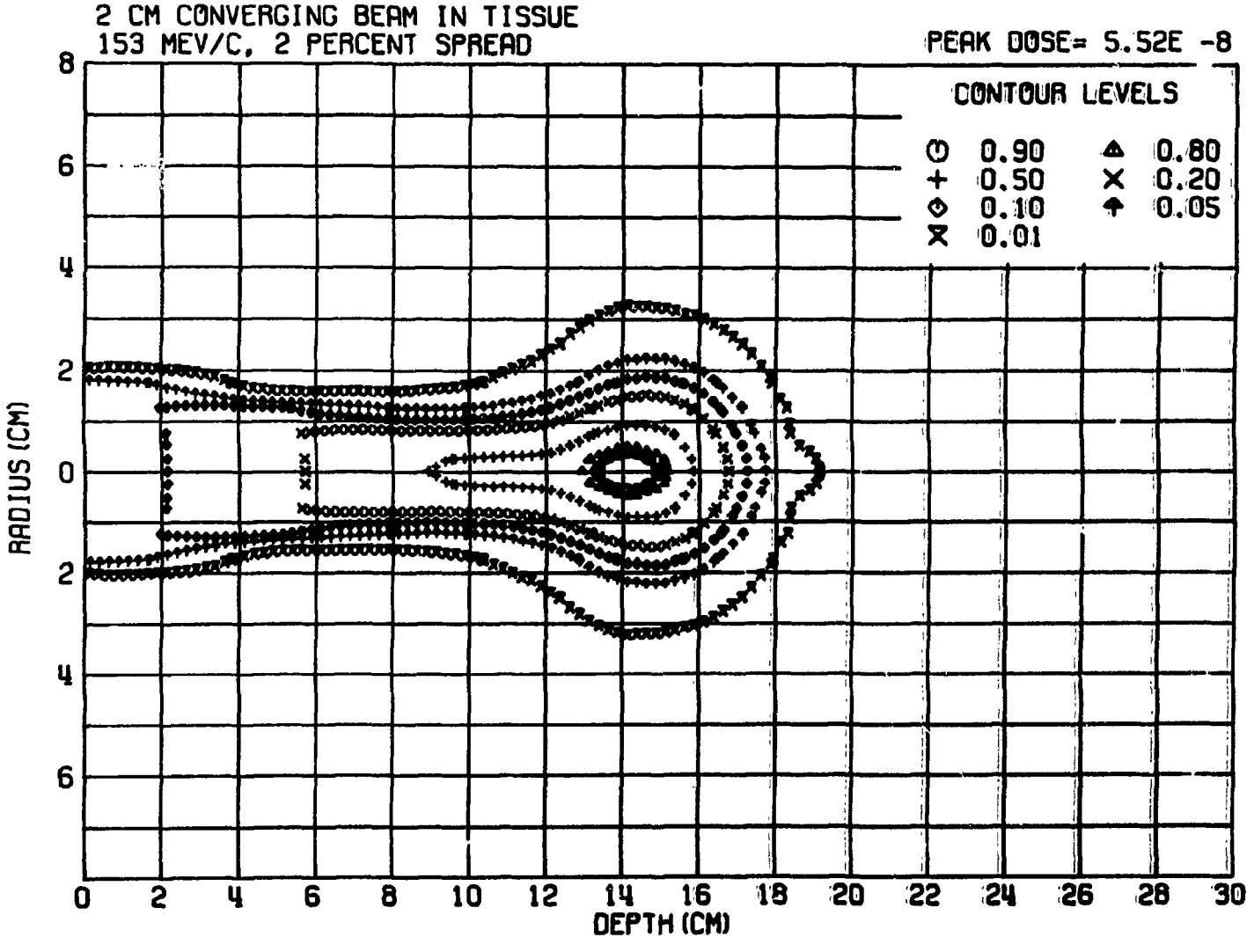

Fig. 16 - Isodose contours for convergent beam indicent on homogeneous soft-tissue target.

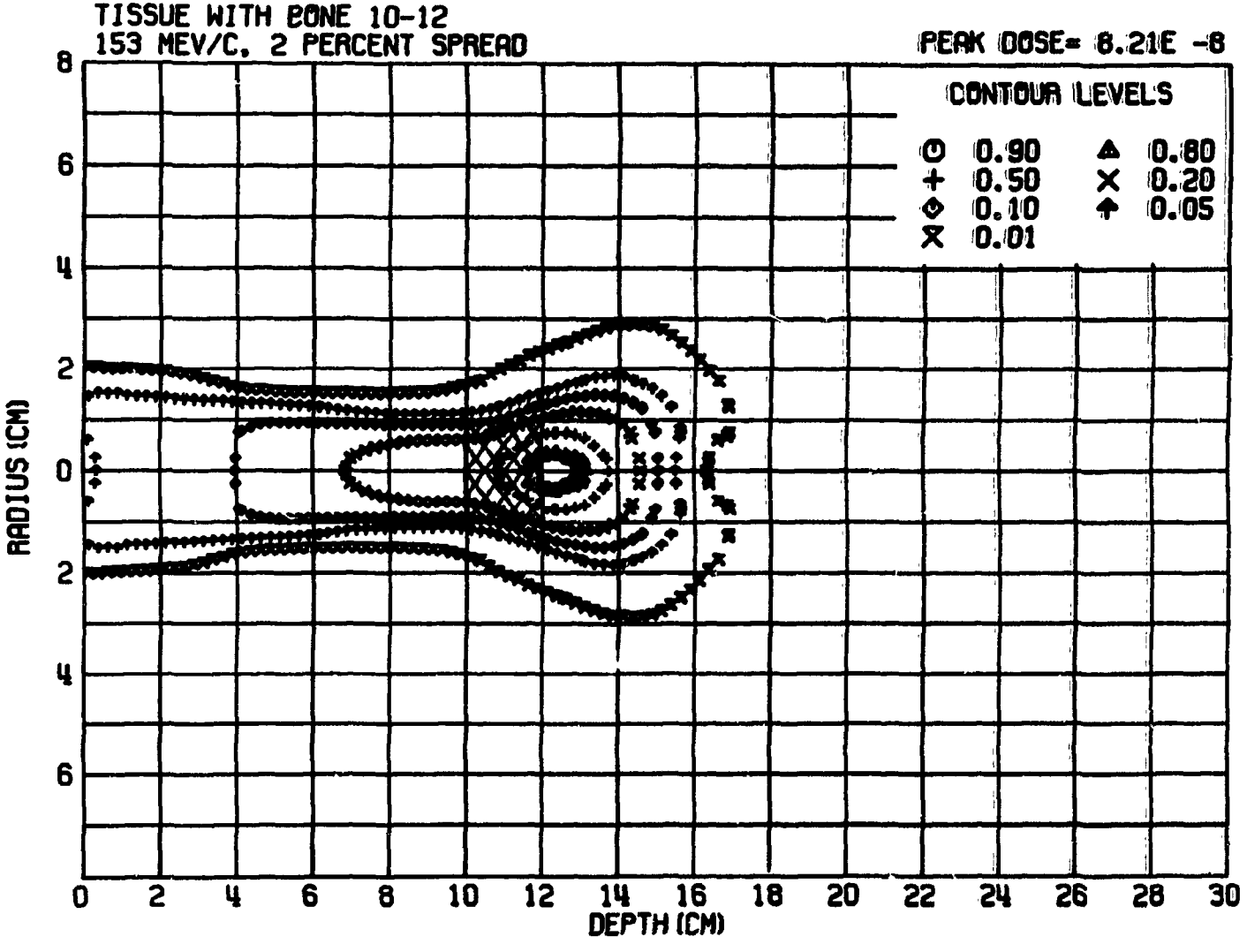

Fig. 17 - Isodose contours for convergent beam with bone cylinder of radius 1 cm between 10 and 12 cm.

ORNL-DWG 75-12570

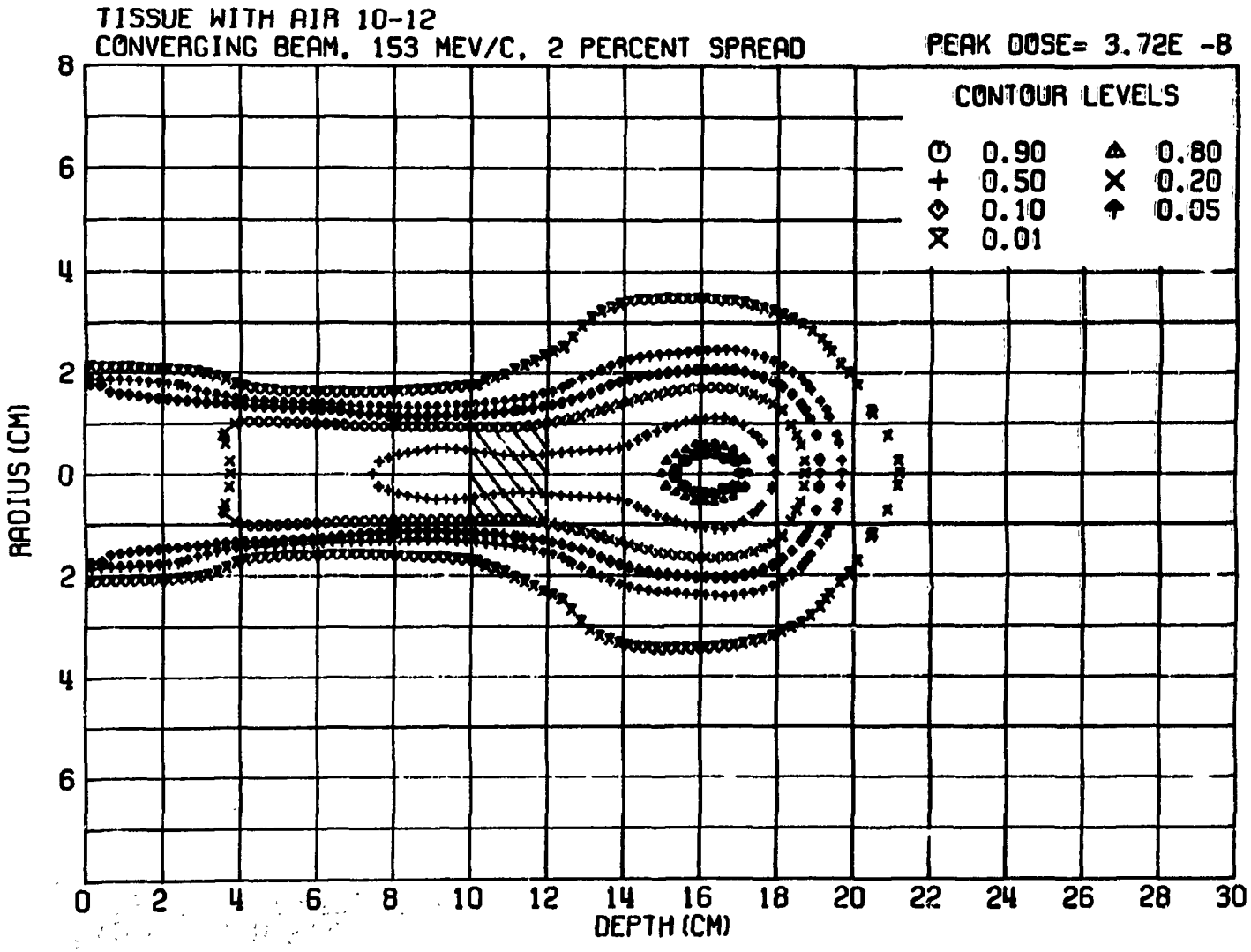

Fig. 18 - Isodose contours for convergent beam with air cylinder of radius 1 cm between 10 and 12 cm.

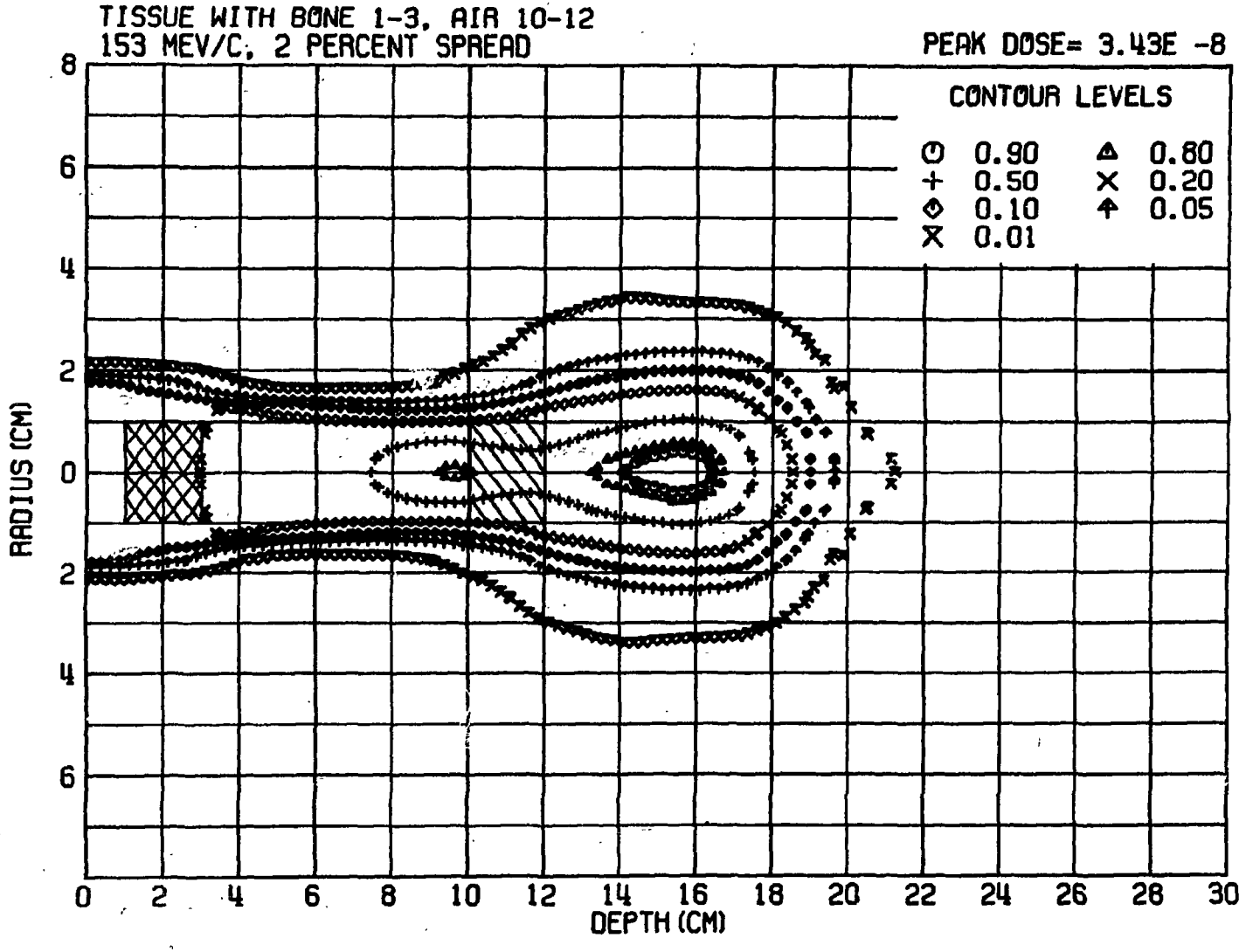

Fig. 19 - Isodose contours for convergent beam with bone cylinder between 1 and 3 cm and air cylinder between 10 and 12 cm.

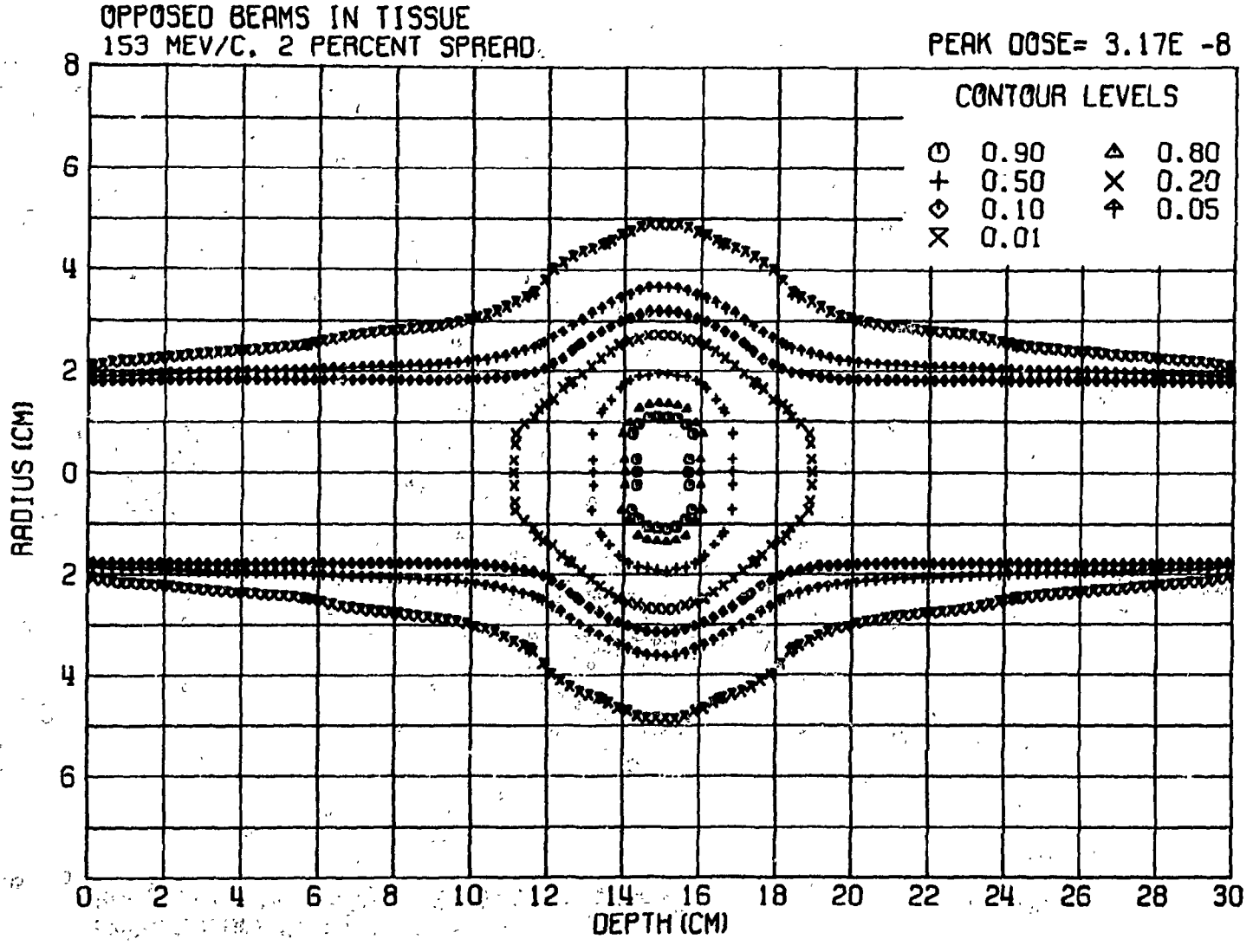

Fig. 20 - Isodose contours for opposed parallel beams on homogeneous soft-tissue target.

ORNL-DWG 75-12573

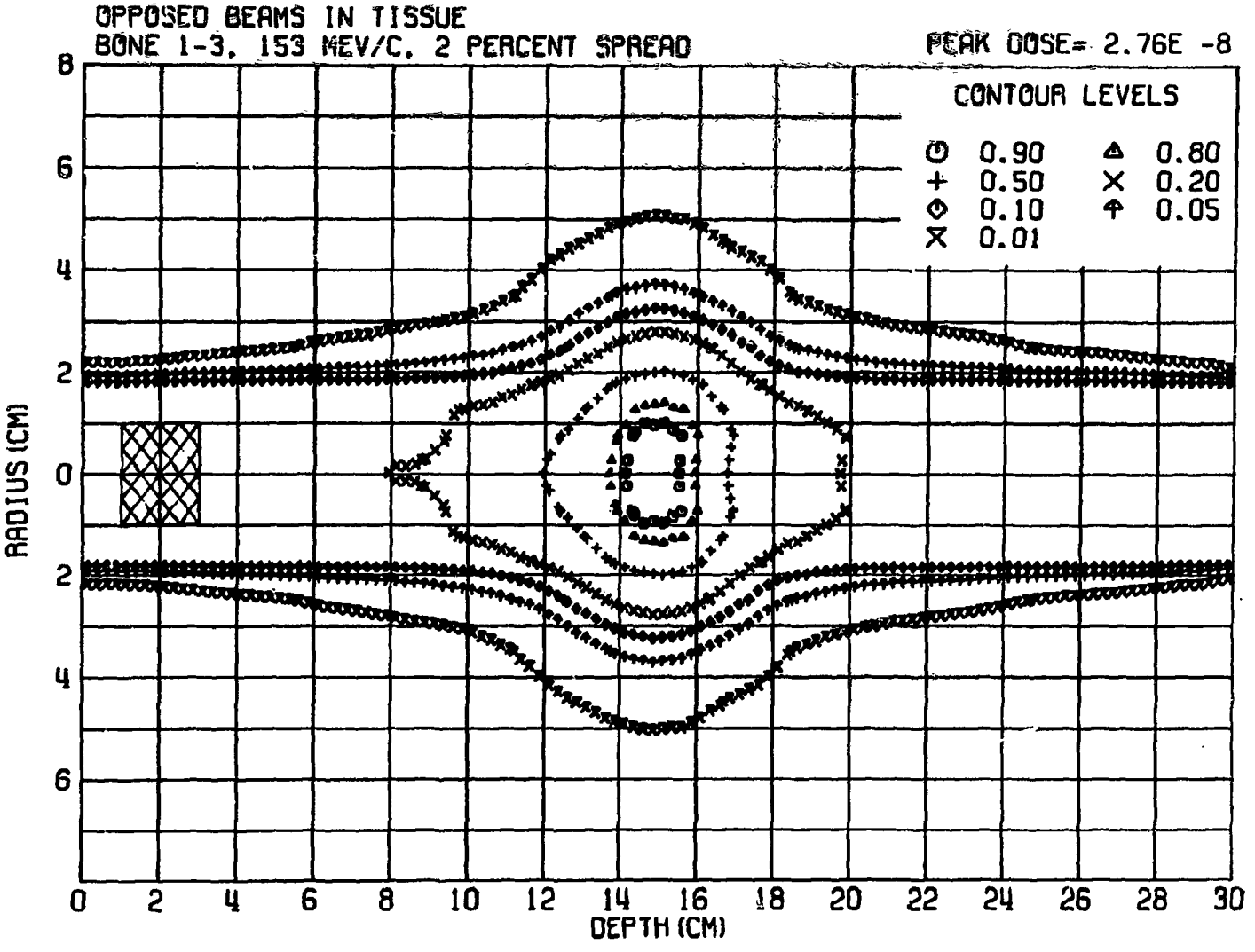

Fig. 21 - Isodose contours for opposed parallel beams with bone cylinder of radius 1 cm between 1 and 3 cm.

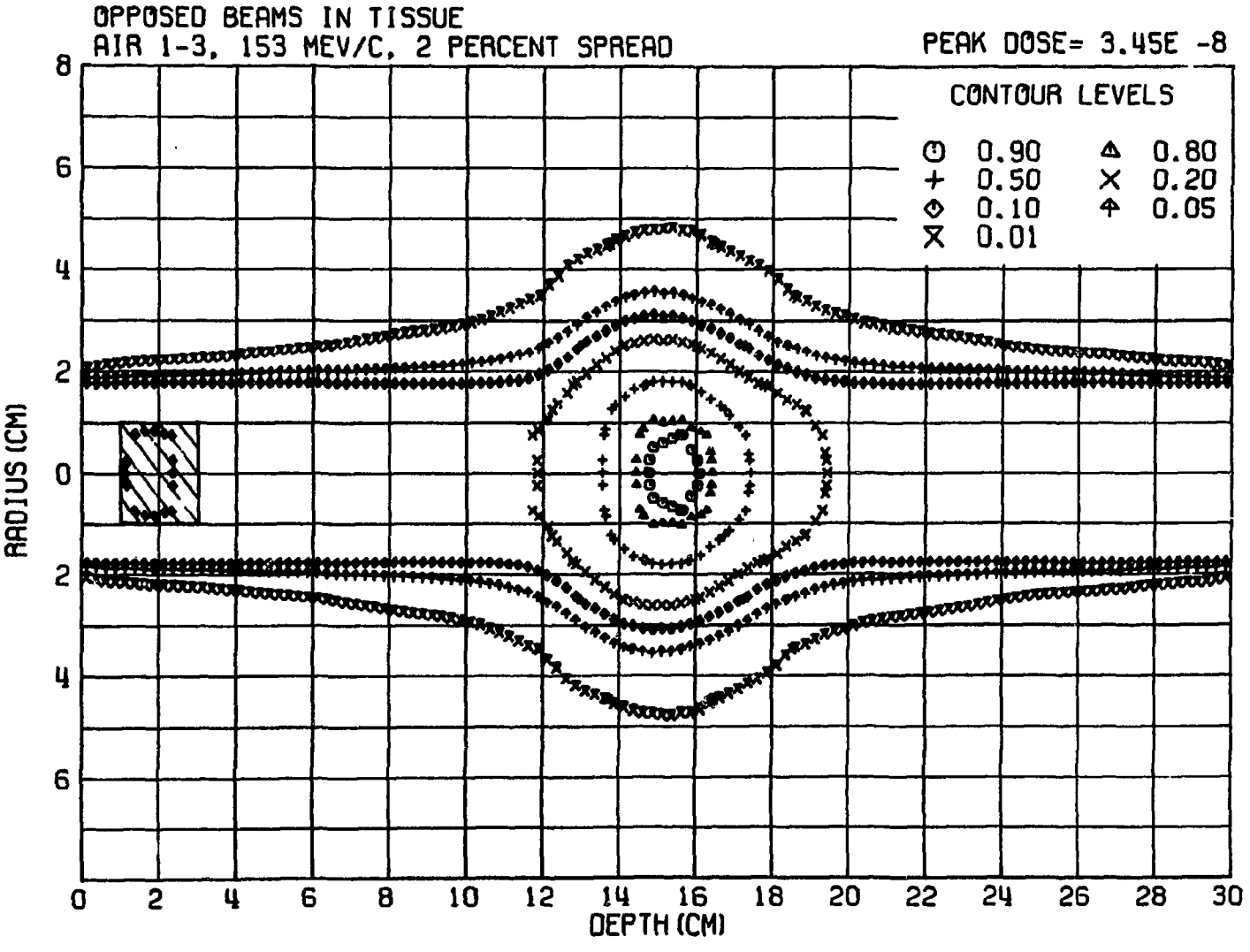

Fig. 22 - Isodose contours for opposed parallel beams with air cylinder of radius 1 cm between 1 and 3 cm.

REFERENCES

Wright, H. A., Hamm, R. N., and Turner, J. E., 1975, to be submitted to Rad. Res.

Turner, J. E., Dutrannois, J., Wright, H. A., Hamm, R. N., Baarli, J. Sullivan, A. H., Berger, M. J., and Seltzer, S. M., 1972, Rad. Res. 52, 229.

Anderson, V. E., Hamm, R. N., Turner, J. E., Wright, H. A., Alsmiller, R. G., Jr., and Armstrong, T. W., 1974, Report ORNL-TM-4296, Oak Ridge National Laboratory, Oak Ridge, TN 37830.

Turner, J. E., Anderson, V. E., Wright, H. A., Snyder, W. S., and Neufeld, J., 1968, Rad. Res. 35, 596.

Santoro, R. T., Alsmiller, R. G. Jr., and Chandler, K. C., 1974, Report ORNL-TM-4407, Oak Ridge National Laboratory, Oak Ridge, TN 37830.

Hamm, R. N., Wright, H. A., and Turner, J. E., 1975, Journ. Appl. Phys., in press.

Nestor, C. W., Jr., Chandler, K. C., Gove, N. B., and McDowell, J. D., 1974, Report ORNL-4596, Oak Ridge National Laboratory, Oak Ridge, TN 37830.